Available online at www.sciencedirect.com
ScienceDirect
Polymer 48 (2007) 564–573
polymer
www.elsevier.com/locate/polymer

Microstructural evolutions of LDPE/PA6 blends by rheological and rheo-optical analyses: Influence of flow and compatibilizer on break-up and coalescence processes

G. Filippone*, P.A. Netti, D. Acierno

Department of Material Engineering and Production, University of Naples Federico II, Piazzale Tecchio 80, 80125 Naples, Italy

Received 12 July 2006; received in revised form 24 November 2006; accepted 27 November 2006
Available online 14 December 2006

Abstract

In this paper we investigate the relationships between flow and morphology in immiscible diluted non-Newtonian (LDPE and PA6) blends. Both rheological and rheo-optical techniques have been used. The effect of a steady shear flow on the blend microstructure has been studied at various shear rates. Moreover, the effects of a compatibilizing agent on rheology and morphology have been analysed. The compatibilizer causes decrease of average drop sizes and stabilization of the blend morphology during a steady shear flow. An attempt to relate the evolution of the volume-average radius with flow has been carried out by following the approach generally pursued for Newtonian polymer blends. The rescaling of both the capillary number and the viscosity ratio by using the shear-rate-dependent viscosity of blend constituents allows to roughly estimate the shear rate wherein severe drop break-up phenomena occur for the uncompatibilized system. Conversely, quantitative discrepancies between experimental data and theoretical expectations have been found for compatibilized blend. The coarsening behaviour in the early stages of an annealing process at rest has been studied, and simple model has been proposed to describe the volume average drop radius growth rate. The coalescence suppression detected for the compatibilized blend could be due to the shielding effect related to the presence of the copolymer layers at the interface between the phases.

Keywords: Non-Newtonian polymer blend; Flow-induced microstructure; Rheo-optical analysis

1. Introduction

Polymer blending has gained much interest in the last years because it offers a simple way to tailor the properties of a polymeric material without investing in new chemistry. Polymer blends constitute over 30% of polymer consumption, and with an annual growth rate of about 9%, nearly constant in the last years, their role in the polymer industry can only increase [1]. Immiscible liquid–liquid suspensions are frequently encountered in food processing, pharmaceutical manufacturing, cosmetic field and plastic technology. The final properties of an immiscible polymer blend strongly depend on its morphology. The rheology of blend constituents and the flow history determine the small-scale arrangement of the phases. The microstructure of a blend affects its rheological, optical and transport properties. The interplay between flow and morphology of a blend results complex, and there might be flow conditions in which multiple steady-state morphology can exist [2]. Further complications occur when either the blend constituents are non-Newtonian or compatibilizing agents are added to the blend. The control and the prediction of the blend morphology is therefore of great importance, and the accurate setting of the flow conditions experienced by the material during the process represents a critical issue.

The flow-induced morphology evolution of polymer blends has been the subject of many studies, and several successes of theories have been pursued in understanding the microstructural changes and the rheological features of such complex

* Corresponding author. Tel.: +39 081 7682407; fax: +39 081 7682404.
E-mail address: gfilippo@unina.it (G. Filippone).

0032-3861/$ - see front matter © 2006 Elsevier Ltd. All rights reserved.
doi:10.1016/j.polymer.2006.11.050

fluids. Two opposite processes determine the morphology of an immiscible polymer blend: break-up and coalescence. If the flow exceeds a critical value, the drops break-up and the average drop size decreases. Conversely, the collision of pairs of droplets can result in their coalescence, causing coarsening of the blend microstructure. The use of emulsion models allows studying the morphology of a polymer blend by analysing its linear viscoelastic spectrum [3,4]. Although these theories can be derived for a distribution of droplet sizes, the use of the volume-average droplet radius, R_V, is generally considered sufficient to describe the blend microstructure. In the previous years, rheo-optical techniques have supplied a powerful tool for the study of flow-induced morphology of multiphase systems directly during flow.

The dynamics of Newtonian drops in Newtonian matrices have been deeply investigated since the pioneering investigations by Taylor [5,6]. The approach classically pursued in order to relate flow and morphology of polymer blends reduces to the analysis of two dimensionless parameters, i.e. the capillary number, $Ca = \eta_m \dot{\gamma} D/2\Gamma$, and the viscosity ratio, $p = \eta_d/\eta_m$. Here D is the droplet diameter, Γ is the interfacial tension, η is the shear viscosity, and the subscripts "m" and "d" refer to the matrix and the dispersed phase, respectively. In extreme synthesis, at a fixed p, the drop will break-up when a critical capillary number, Ca_{cr} will be reached. The master curve for single drop break-up is usually referred to as the Grace's curve [7]. Several authors have tried to recover a simple relationship for either non-Newtonian blends or concentrated emulsions [8–10], but lack of theories and constitutive model still exist for such systems. Moreover, the use of compatibilizing agents, often employed to stabilize the morphology of the blends [11,12], introduces further complications to the definition of general rules able to relate the material characteristics and the process conditions to the final blend morphology.

The overall objective of this study is to investigate the relationships between flow and morphology of diluted LDPE/PA6 (97/3 wt/wt) with and without compatibilizer. The steady and dynamic flow behaviour of materials was studied by means of a rotational rheometer. The microstructure of the blends was investigated through a rheo-optical apparatus. First, the effect of a steady flow field was investigated qualitatively, by analysing the evolution of drop size distributions as a function of the shear rate and of the presence of the compatibilizer. Then, an attempt to relate the flow to the final blend phase morphology was carried out starting from the classical approaches. In spite of the low dispersed phase concentration of studied blends, some coalescence phenomena have been detected during rheo-optical investigations. Coalescence makes difficult to get fine polymer blend microstructures. It was shown that a dispersed phase concentration of 0.5–1 wt% can give rise to flow-induced coalescence phenomena [13]. A quiescent annealing process can cause coarsening of the blend morphology because of interfacial relaxation. The drop size growth is faster at the beginning of the annealing, and it progressively decreases with time. The coalescence process in state of rest was investigated, and a simple model was derived for the coarsening rate.

2. Experimental

2.1. Materials and blending

The blend investigated in this work consisted of a low-density polyethylene (LDPE) as continuous phase, and a polyamide (PA6) as dispersed phase. The LDPE (*Riblene FF20*, kindly supplied by Polimeri Europa, Milano (Italy)) has a molecular weight of about 50.000 g/mol, a density of 0.922 g/cm^3 at 23 °C and MFI of 0.8 g/10 min at 190 °C. The PA6, kindly supplied by Snia Tecnopolimeri (Milano, Italy), has a molecular weight of about 17.000 g/mol, a density of 1.13 g/cm^3, an intrinsic viscosity of 1.45 dL/g (measured at 25 °C in 85% formic acid) and contents of amine and carboxyl end groups of 34 and 35 meq/kg, respectively. An ethylene–acrylic acid copolymer (*ESCOR 500*, supplied by Exxon-Mobile Chemical Mediterranea) was used as compatibilizer. It contains 6% of acrylic acid and it has a MFI of 0.2 g/min at 190 °C. ESCOR 500 acts as compatibilizing agent by promoting strong interactions between free carboxylic groups of the copolymer and functional amide and amine groups of PA6. These interactions cause the reduction of the interfacial tension owing to the contemporaneous presence of two functional groups: the ethylene, interacting with the polyethylene matrix, and the free carboxylic groups, miscible in the dispersed polyamide phase. A good compatibilization efficiency of Escor 5001 has been noticed from X-ray studies, optical and scanning electron microscopy and microhardness measurements performed upon blends constituted by the same polymers used in this work [14–16]. The addition of 1 phr of Escor causes a reduction of interfacial tension of about 35% respect to the uncompatibilized blend.

Blends of LDPE, PA6 and the compatibilizer were prepared by the following procedure. Pellets of LDPE and PA6 in a 97/3 wt/wt ratio, previously dried at 90 °C for 16 h, were blended into a Haake mixer (Rheocord 600p) at 240 °C and 30 rpm. For compatibilized systems, an amount of 1 phr of Escor 5001 was added. The blends were mixed for about 4 min until a constant torque at the rotor axis was reached, and the materials were quenched in cold water at the end of the process. A reasonable extent of the grafting reactions of compatibilizer has been found for these mixing conditions [17]. The sample compositions are summarized in Table 1 together with the interfacial tensions as derived by Minkova et al. through the breaking thread method [18].

2.2. Characterization and data analysis

A strain-controlled rotational rheometer was used for rheological experiments (mod. ARES L.S., Rheometric Scientific™). All tests were carried out by using 25 mm parallel plates in inert atmosphere (gaseous nitrogen) at $T = 240$ °C. Linear dynamic measurements (strain amplitude of 2%) were performed in order to investigate the rheological behaviour in oscillatory flow. The range of investigated frequencies was from $\omega = 0.1$ to 100 rad s^{-1}. Linearity checks have shown that the viscoelastic behaviour of the blends to be linear up to

Table 1
Blend compositions and interfacial tensions

Blend composition [wt%]	Code name	Interfacial tension (mN/m)
LDPE/PA6 100/0	P1	–
LDPE/PA6 0/100	P2	–
LDPE/PA6 97/3	P12	0.0125[a]
LDPE/PA6/Escor 5001 97/3/1 phr	P12E	0.0075[a]

[a] Data from Minkova et al. [18].

strain amplitude of 7% for all the frequencies used. Due to the onset of melt-fracture phenomena occurring at high shear rates, the steady-state shear behaviour was investigated by testing the materials from $\dot{\gamma} = 0.1$ to 15.85 s^{-1}. The measurement time was established by monitoring the transient stress, $\sigma(t)$, in step rate experiments. A strain $\gamma = \dot{\gamma}t = 100$ was found to get quite stable stress profiles.

A Cambridge Shearing System CSS450 (Linkam™) was employed to investigate the evolutions of blend morphology soon after a steady shear flow. The apparatus consists of a rotating 30 mm parallel-plate device coupled with an optical microscope (mod. Axioskop 2, Carl Zeiss Inc.). The lower slide connected to a motor is able to submit the sample to various flow fields. The samples were submitted to steady shear flows from 0.0631 s^{-1} to 1.585 s^{-1}. Relevant droplet break-up phenomena occurring at higher shear rates cause a reduction in image definition when focusing inside the samples, making difficult the subsequent image analyses. The duration of the flows was set to get strains comparable with those of rheological measurements. Stopped the flow and waited few seconds for the drops to retract their spherical shape, it has been provided to the image acquisition. A camera (Pulnix TMC-76S) connected to a digital acquisition board (Frame Grabber PCI-1409) captured the images of the samples after flow. Observations were performed in transmitted light by using various combinations of objective lenses. The micrographs were subsequently analysed by means of a software for droplet recognition and measurement. The basic steps of image analysis are detection of droplet edges, removing of continuous phase and measurement of particle sizes. Although the duration of rheo-optical analyses was contained within a maximum of ~200 s, some quiescent coarsening process has been detected during the image acquiring. Therefore, investigations were performed to evaluate the drop size evolutions at rest by monitoring the blend morphology during annealing at 240 °C.

In order to get reliable information about the morphology of the blends, a statistical analysis was performed on drop size data. Many drops were measured by analysing various images for each test condition. Moreover, more than one image was acquired at different depths within the same sample. In agreement with the results of Caserta et al. [19], the drop sizes were found to be quite uniform throughout the sample thickness. Considering that each blend micrograph contains on average 30/100 dispersed PA6 domains, about 500 droplets were measured for each test condition. The Paine's approach was adopted in order to estimate the sampling error [20]. For particle systems with log-normal distribution of particle diameters, a critical number of object, N_{crit}, has to be sampled to avoid dramatic sampling error:

$$N_{crit} = \exp[1.5 + 5.5\ln(GSD) + 7.5\ln^2(GSD)] \quad (1)$$

where GSD is the geometrical standard deviation of the log-normal distribution. When $N > N_{crit}$, particles have been sampled, the percentage error in the volumetric mean diameter D_v can be reliably estimated, while for $N < N_{crit}$ the GSD is seriously and systematically underestimated. The geometrical standard deviation of our samples was found to vary between 1.4 and 1.7, leading to values of N_{crit} from ~10^2 to ~10^3 to be in the Paine's acceptable region. The data were rejected when $N < N_{crit}$ drops were available and further experiments were performed.

3. Results and discussion

3.1. Steady shear behaviour

The steady response of Newtonian blends at low shear rate and low volume fraction is well described by the model of Choi and Schowalter, predicting an increase of the blend viscosity with respect to the neat matrix whatever the viscosity of the dispersed phase [21]. The steady-state shear behaviour of non-Newtonian polymer blends is more complex: the viscosity may follow a logarithmic mixing rule ($\log \eta = \sum \Phi_i \ln \eta_i$), or it may fall well below the mixing rule [21,22].

The viscosities of the blends and pure constituents are shown in Fig. 1.

A pseudo-Newtonian plateau characterizes the flow behaviour of PA6, while the LDPE is shear-thinning in the range of shear rates investigated. This causes the crossover of the viscosity curves of blend constituents at $\dot{\gamma} \sim 7\ s^{-1}$, making the viscosity ratio p dependent on the shear rate.

The flow curves of the blends are rather similar to those of the LDPE. The presence of the PA6 second phase causes a vertical shift of the curves without significantly affecting the shear-rate dependence of the viscosity. The blend P12 follows

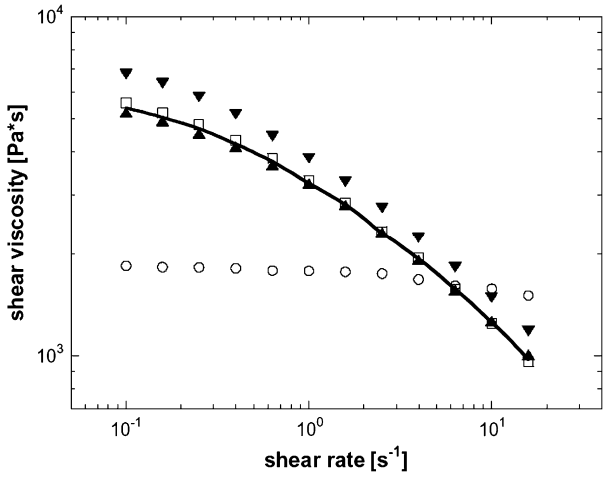

Fig. 1. Steady shear viscosities of blends (▲ P12, ▼ P12E) and pure components (□ P1, ○ P2). The solid line is the prediction of the log-additivity rule.

quite well the log-additivity rule, indicated by the solid line. The compatibilized system shows positive deviations from the log-additivity rule in the whole range of investigated shear rates. The increase of the viscosity with respect to the pure LDPE matrix can be attributed to several reasons, such as the enhancing of the dispersion promoted by the compatibilizer, the increase of the total apparent volume of the dispersed phase due to the compatibilizer layer attached to the drop surfaces, the increase of interaction among the droplets and the stiffening of the interface.

3.2. Linear viscoelastic behaviour

The linear viscoelastic behaviour of an immiscible polymer blend during oscillatory flow shows an additional relaxation process at low frequencies related to the tendency of the droplets to relax back to a spherical shape under the influence of interfacial tension. The time scale of such a process is $\tau_D \propto R\eta_m\Gamma$. If the elastic relaxation times of the matrix and droplet fluids are much shorter than τ_D, then the droplet contribution will appear as a shoulder at low frequencies in a log–log plot of the storage shear modulus G' vs. ω. The presence of the droplets has only a small effect on the loss shear modulus G''. The response of a polymer blend at high frequencies draws down from the direct contribution of the components [23].

The linear viscoelastic moduli of the blends and pure constituents are shown in Fig. 2 as a function of frequency.

At high frequencies, the data reported in Fig. 2 follow the same trend of steady shear viscosity, the moduli of the blends being higher or lower than those of the LDPE, respectively depending on the presence or absence of the compatibilizing agent. However, the dependence of G' on ω for both blends at low frequencies becomes weaker than that of pure LDPE matrix, as shown in detail in the insets of Fig. 2. This indicates the emergence of additional elasticity related to the perturbation of the shape of the dispersed phase.

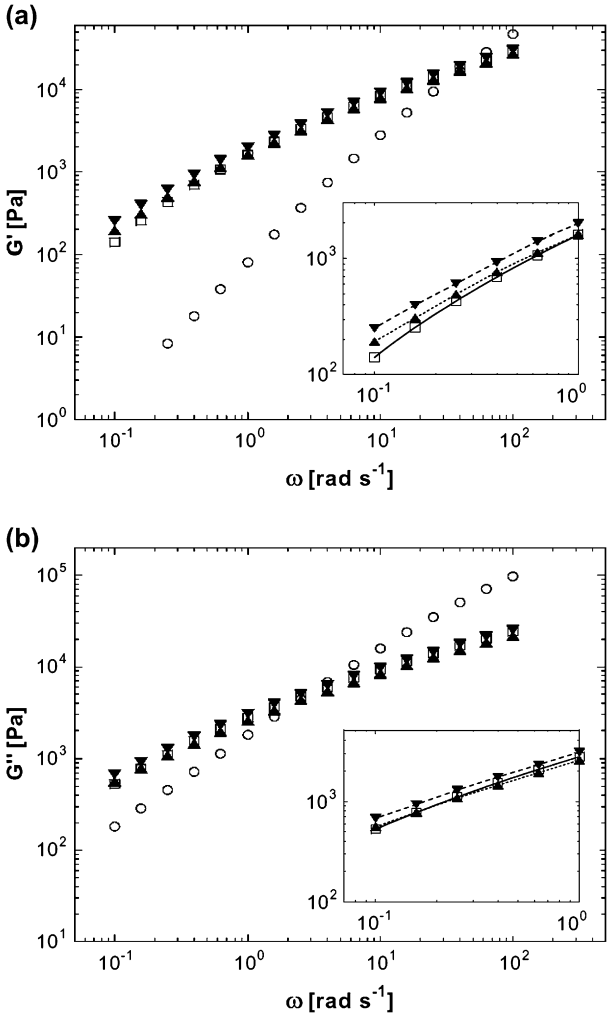

Fig. 2. Dynamic storage (a) and loss (b) moduli as a function of frequency for blends (▲ P12, ▼ P12E) and pure components (□ P1, ○ P2). The magnifications of $G'(\omega)$ and $G''(\omega)$ at low frequencies are reported in the insets.

3.3. Evolution of drop size distributions after flow – results

The drop size distributions in state of rest for blends P12 and P12E are shown in Fig. 3, together with the micrographs of the samples. The compatibilizer causes the decrease of the volumetric mean diameter from $D_v \approx 13.9$ μm (P12) to $D_v \approx 10.1$ μm (P12E). The solid lines of Fig. 3 have been obtained by fitting a log-normal distribution to the experimental data.

Two opposite processes determine the average size of a group of droplets subjected to a steady shear flow: break-up and coalescence. The evolutions of the cumulative drop size distributions soon after steady shear flows at various shear rates are reported in Fig. 4. The volumetric mean diameters after each flow are summarized in Table 2.

A broadening of the P12 size distribution mainly occurs after the flow at lowest shear rate. Such a feature draws from the concomitance of break-up and coalescence processes, making the average drop size almost constant in such a weak flow field. With increasing the shear rate, the flow starts to clearly affect the P12 blend microstructure and the PA6 drop size distributions progressively shifts toward small diameters, indicating more and more relevant drop break-up phenomena. Interestingly, this trend is coupled with the appearance of big diameter tails at the highest shear rate. The emerging of such positive skewness suggests the occurrence of coalescence phenomena overlapping to the break-up process, as a consequence of the poor stability of too small PA6 droplets in the blend without compatibilizer. The compatibilizer causes stabilization of the microstructure after shear flows up to $\dot{\gamma} = 0.251\ s^{-1}$. Above this value, the drop size distributions get narrow and evolve toward smaller diameters with increasing shear rate. The lowering of interfacial tension ensured by the compatibilizer stabilizes the small PA6 droplets at high shear rates, and the absence of big diameter tails at high shear rates suggests the absence of relevant coalescence phenomena observed for the blend P12.

Finally, the polydispersity indices (D_v/D_n) of the blends are in the range of 1.1–1.5. For the sake of simplicity, we assume

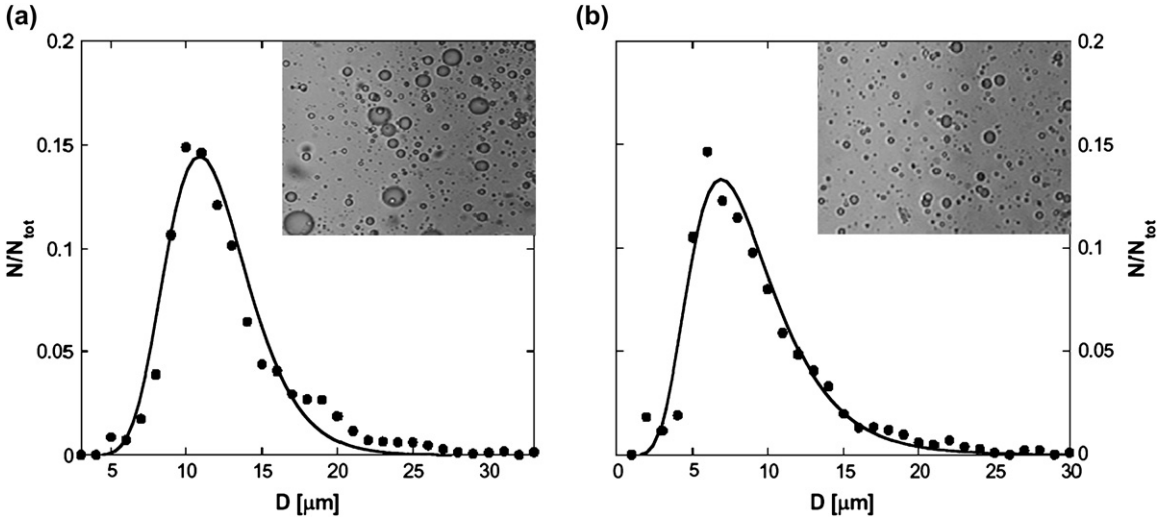

Fig. 3. Drop size distributions and micrographs of P12 (a) and P12E (b) samples before any flow. The solid lines represent the best fit of experimental data with a log-normal distribution. Two micrographs of the samples are shown in the insets.

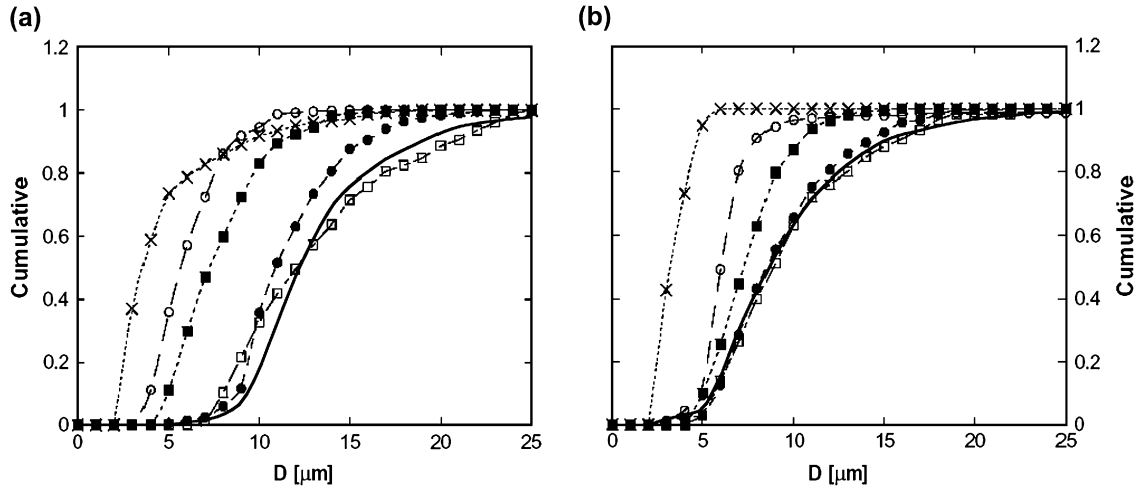

Fig. 4. Cumulative drop size distributions for P12 (a) and P12E (b) blends soon after steady shear flows at $\dot{\gamma} = 0.063\ s^{-1}$ (□), $0.1\ s^{-1}$ (●), $0.251\ s^{-1}$ (■), 0.631 (○) and $1.585\ s^{-1}$ (×). The solid lines represent the cumulative size distributions of the samples before any flow.

our materials as systems of randomly distributed monodisperse spherical particles with radius R_v.

3.4. Evolution of drop size distributions after flow — discussion

In order to reach a better understanding of the break-up and coalescence mechanisms governing the flow-induced blend microstructure, the two processes have to be analysed separately.

Table 2
Volumetric mean diameters after steady shear flows at various shear rates

	P12		P12E	
Shear rate (1/s)	D_v (μm)	GSD	D_v (μm)	GSD
Rest	6.98	0.90	5.05	0.77
0.063	7.00	1.03	5.03	0.87
0.1	5.30	0.51	5.00	0.68
0.251	4.90	0.69	3.90	0.58
0.631	4.01	0.67	2.77	0.56
1.585	1.81	0.52	1.64	0.48

The viscosity ratio and the capillary number govern the flow-induced break-up process. For a single Newtonian droplet, the plot of Ca_{cr} vs. p gives a critical curve for break-up with a vertical asymptote for $p \sim 4$ [7]. de Bruijn derived the following semiempirical equation for the limiting curve for break-up [24]:

$$\log Ca_{cr} = -0.506 - 0.0995 \log p + 0.124(\log p)^2 - \frac{0.115}{\log p - \log 4.08} \quad (2)$$

For very diluted blends, the steady drop size gives a capillary number close to the critical value for break-up, Ca_{cr}. For Newtonian diluted blends, in which η_m is independent on the shear rate, this means that when morphological equilibrium is reached, the equilibrium droplet radius R scales with $\dot{\gamma}^{-1}$.

The break-up process competes with coalescence phenomena during flow. In order for two drops coalesce into one, they must collide for a time large enough to make possible the drainage of the matrix film between the approaching droplets. During a shear flow, the duration of collision can be set to $\dot{\gamma}^{-1}$, while different expressions for the drainage time have been proposed depending on the interfacial mobility (fully mobile interface, FMI, suitable when $p \ll 1$; partially mobile, PMI, proper for $p \sim 1$; immobile interface, IMI, appropriate when $p \ll 1$) [25–27]. By equating the drainage time to the collision time, one gets an expression for the critical drop size below which coalescence occurs. The following limiting curves have been obtained:

$$\text{FMI} \quad R \ln\left(\frac{R}{h_c}\right) = \frac{2}{3}\frac{\Gamma}{\eta_m \dot{\gamma}} \tag{3}$$

$$\text{PMI} \quad R = \left(\frac{4}{\sqrt{3}}\frac{h_c}{p}\right)^{0.4}\left(\frac{\Gamma}{\eta_m \dot{\gamma}}\right)^{0.6} \tag{4}$$

$$\text{IMI} \quad R = \left(\frac{32}{9}\right)^{0.25}\left(\frac{h_c \Gamma}{\eta_m \dot{\gamma}}\right)^{0.5} \tag{5}$$

In the previous expressions, h_c is the critical distance between the drops at which the matrix film separating the particles breaks and coalescence occur. The distance h_c depends on Van der Waals forces and is approximated to $h_c = [(AR)/(8\pi\Gamma)]^{1/3}$, where A is the Hamaker constant [26].

Once the shear rate is fixed, the flow is able to break only droplets with diameter greater than a critical value. On the other hand, two drops can only coalesce if their average size is smaller than a critical one. The minimum drop size for break-up and the maximum drop size for coalescence does not coincide. The limiting break-up and coalescence curves overlay at a critical shear rate, $\dot{\gamma}_{cr}$, above which the blend microstructure is a unique function of shear rate. Multiple pseudo-steady states are instead possible below $\dot{\gamma}_{cr}$ depending on the flow history [2].

The previous limiting curves for break-up and coalescence do not consider any shear-rate dependence of the blend constituents. This makes Eqs. (2)–(5) unsuitable for the blends studied in this work, due to their markedly shear-thinning behaviour.

Jensen et al. showed experimentally that the critical capillary number in simple shear flow decreases with increasing droplet concentration. Their break-up data are well described by the single-drop results (Eq. (2)) but with the shear-rate-dependent dispersion viscosity, $\eta_b(\dot{\gamma})$, replacing the matrix viscosity [8]. The rationale for this arises from the assumption that the forces exerted on a single droplet immersed in a concentrated emulsion is approximately proportional to the viscosity of the surrounding emulsion (mean field approximation). Furthermore, the Jansen's approach allows take into account the shear-thinning behaviour of their concentrated emulsions.

The shear-rate dependence of the blends studied in this work arises from the intrinsic non-Newtonian feature of both the pure constituents. The simplest way to account for this is to rescale the limiting break-up and coalescence curves by using the shear-rate-dependent viscosities of both the matrix, $\eta_m(\dot{\gamma})$, and the dispersed phase, $\eta_d(\dot{\gamma})$.

The rescaled values of the viscosity ratio vary between 0.35 and 1.5 for P12 and between 0.27 and 1.27 for P12E. In these ranges, the limiting break-up curve is rather flat (see Eq. (2)), and the common value of $Ca^* = 0.717$ was used to derive the equilibrium droplet radius R:

$$R = \frac{Ca_{cr}(\dot{\gamma})\Gamma}{\eta_m(\dot{\gamma})}\frac{1}{\dot{\gamma}} \cong \frac{0.717\Gamma}{\eta_m(\dot{\gamma})}\frac{1}{\dot{\gamma}} \tag{6}$$

The shear-thinning behaviour of the matrix reduces the scaling dependence $R \propto \dot{\gamma} - 1$ of Newtonian blends. Moreover, the presence of the compatibilizer causes lowering of the limiting break-up curve as a consequence of the lowering of interfacial tension Γ.

The rescaled viscosity ratio for both the blends varies around 1, suggesting the rescaling of the PMI limiting curve for coalescence (Eq. (4)), at least for the blend P12. On the other hand, the employ of Eq. (4) could be inadequate for the blend P12E, in which a decrease in mobility of the interface occurs due to the drag of compatibilizer molecules to the periphery approaching areas of the droplets (Marangoni effect) [28,29]. This mechanism has qualitatively the same influence on the matrix drainage as an increase in viscosity of the dispersed phase. Therefore, for P12E blend we propose the rescaling of the IMI limiting curve for coalescence (Eq. (5)).

After all, the equilibrium drop radii derived by the rescaled Eqs. (4) and (5) are

$$R = \left(\frac{4}{\sqrt{3}}\frac{h_c}{\eta_d(\dot{\gamma})/\eta_m(\dot{\gamma})}\right)^{0.4}\left(\frac{\Gamma}{\eta_m(\dot{\gamma})\dot{\gamma}}\right)^{0.6} \quad \text{(for P12)} \tag{7}$$

$$R = \left(\frac{32}{9}\right)^{0.25}\left(\frac{h_c \Gamma}{\eta_m(\dot{\gamma})\dot{\gamma}}\right)^{0.5} \quad \text{(for P12E)} \tag{8}$$

Eqs. (6)–(8) express the equilibrium droplet radius as a function of shear rate. In order to test the previous scaling models, we used the results of rheo-optical analysis discussed before by considering the volume-average drop radius as representative of the blends.

The volume-average radii of the blends, R_v, soon after the shear flows at various shear rates are reported in Fig. 5 together with the rescaled limiting break-up and coalescence curves (Eqs. (6)–(8)). For the sake of simplicity, the common typical value for polymer blends of $h_c = 10^{-8}$ m was used in Eqs. (7) and (8).

The low shear rate data of P12 blend fall in the hysteresis region, where droplets too small to break-up and too large to coalesce coexist. In spite of some broadening of drop size distributions, the average size of domains is quite stable in this region. Once the limiting break-up curve is reached, relevant break-up phenomena occur and the R_v decreases following the rescaled critical curve for break-up.

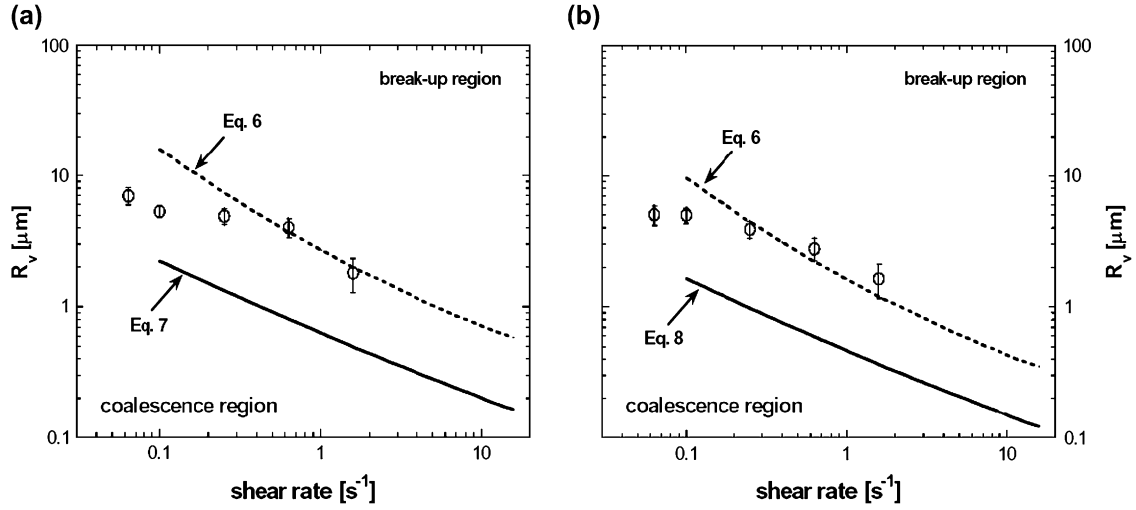

Fig. 5. Volumetric mean radii of P12 (a) and P12E (b) blends soon after shear flows at various shear rates. Solid and dashed lines are the limiting break-up (Eq. (6)) and coalescence curves (Eq. (7) for P12 and Eq. (8) for P12E).

The stabilization of morphology can be argued also for the P12E blend, and relevant changes in drop sizes only occur at high shear rate due to break-up phenomena. Nevertheless, an underestimation of the rescaled break-up curve can be observed for the compatibilized system. The experimental data indicate dependence of R_v on $\dot{\gamma}$ weaker than that predicted by Eq. (6). The presence of the compatibilizer is taken into account by introducing into Eq. (6) a reduced value of the interfacial tension Γ (see Table 1). This causes a simple lowering of the limiting break-up curve, making the scaling model inappropriate to correctly describe the effects of the compatibilizer. The discrepancies emerged between the scaling model and the rheo-optical data may arise from the stiffness of the interphase layer generally proposed to explain the increase of viscosity commonly observed in compatibilized blends [1]. This effect could hinder drop deformation causing a delay of break-up process unpredictable by using Eq. (6).

In conclusion, although some disagreement has been found for compatibilized blend, the rescaling of the capillary number and the viscosity ratio by using the shear-rate-dependent viscosities of blend constituents allows to roughly estimate the shear rates at which relevant break-up phenomena occur. Finally, we observe that a direct consequence of the shear-thinning behaviour of the matrix phase is the flattening of both the rescaled limiting curves. Therefore, the overlay of limiting curves occurs at high shear rates. In other words, a wide range of shear rate in which the domain sizes are not well controlled by the flow characterizes the non-Newtonian blends studied here. It is important to observe that, beside the effects of flow history, the microstructure of the blends in this region will strongly depend also on their initial morphology.

3.5. Coarsening behaviour during quiescent annealing

Provided that a blend is kept prolonged time in the molten state, the size of dispersed phase increases because of interfacial relaxation. The stability of blend microstructure at rest was investigated by monitoring the drop size evolutions at 240 °C as a function of time. The blends were previously submitted to shear flow at high shear rates in order to induce severe droplet break-up phenomena before starting the quiescent annealing process.

The change in the average volume radius per unit time due to coalescence is described by the following equation [30]:

$$\frac{dR_v}{dt} = \frac{\phi p(h) R_v}{3\tau} \tag{9}$$

where ϕ is the volume fraction of droplets with radius R_v, $p(h)$ is the probability that the distance between the surfaces of two droplets is h, and τ is the total coalescence time. In order to evaluate the quiescent coalescence rate, both $p(h)$ and τ have to be determined.

In general, the coalescence mechanisms at rest are described in terms of evaporation–condensation (the so-called Ostwald ripening) or Brownian coagulation processes [30,31]. The coalescence process can be depicted as a sequence of three stages:

1. *Approach* of two particles with radii R_1 and R_2 ($R_1 = R_2 = R$ in the monodisperse case) and formation of a parallel film between the drops with thickness h_0.
2. *Drainage* of the matrix trapped between the drops up to a critical distance h_c for film rupture.
3. Evolution of the 'neck' to a coalesced sphere (*merging*).

The total coalescence time τ is the sum of the durations of each single stage.

Generally, two droplets approach due to Brownian motion, buoyancy and Van der Waals forces. The drops of our blends are large enough so that Brownian motion can be neglected. Moreover, the high zero-shear viscosity of the matrix and the small difference in blend constituent density make buoyancy negligible. On the other hand, Van der Waals forces become relevant when interparticle distances are very small,

i.e. less than 1 μm. The average wall-to-wall distance h in a randomly distributed monodisperse system (diameter D_v) of spherical particles can be estimated as [32]

$$\frac{h}{D_v} = \left(\frac{1}{3\pi\phi} + \frac{5}{6}\right)^{1/2} - 1 \tag{10}$$

For our typical value of $D_v \sim 10$ μm, the wall-to-wall distance is of order of ~ 10 μm, so that not even Van der Waals forces can justify the approach of droplets. Hence, if quiescent coalescence occurs, some alternative mechanism has to be considered to start the coarsening process.

An image of P12 blend in the earlier stage of coalescence at rest is shown in Fig. 6. The presence of two pairs of droplets in contact can be observed. It is interesting to note the flattening of the drop surfaces in the contact zone. The presence of such droplets statistically in contact (i.e., at a distance $h \ll D$) at the beginning of the annealing process could originate the quiescent coalescence process. If this idea holds, the duration of first stage is negligible and the total coalescence time reduces to the sum of drainage and merging times.

The drainage of the matrix trapped between the droplets is the thinning process of the matrix film separating the two contacting droplets. The film thickness decreases from h_0, that is the distance at which a drop ''feels'' another one, to a critical distance h_c for the film break-up. Both Van der Waals forces and diffusion mechanisms have been proposed as the driven processes of film drainage stage [30,33]. The flattening of drop surfaces noticed in Fig. 6 could suggest that the gradients in chemical potential causes non-Fickian diffusion and promotes the film drainage. As soon as the matrix film is drained, the droplets form a dumbbell-like particle that is not in thermodynamic equilibrium. The ''*8-shaped particle*'' retracts to a sphere to minimize the interfacial area. On the other hand, the merging of particles causes a viscous flow within both the droplets and the surrounding matrix. This step will occur only if an energetic gain is reached. The merging time, τ_{merge}, can be thus evaluated by equating the rate of interfacial energy reduction and that of viscous dissipation due to the viscous flow. Yu et al. derived the following relationship [30]:

$$\tau_{merge} = \frac{R\eta^*}{2\sqrt[3]{2\Gamma}} \tag{11}$$

where $\eta^* = \eta_m + 16\eta_d$ is the bulk viscosity of the blend.

The total coalescence time τ of Eq. (9) is given by $\tau = \tau_{approach} + \tau_{drain} + \tau_{merge} \cong \tau_{drain} + \tau_{merge}$. Nevertheless, it has been shown that the drainage stage can be neglected in comparison with the merging stage at the beginning of the annealing process. At the later annealing process, τ_{drain} becomes increasingly important in the coalescence, but it reaches at most the 10% of the total coalescence time [30]. Hence, we propose to roughly set $\tau \cong \tau_{merge}$ into Eq. (9).

Fortenlý and Źivný derived the following expression for the probability distribution function of interparticle distances [34]:

$$p(h) = 1 - \exp\left\{-\frac{9\Phi h}{2(1-\Phi)R}\right\} \tag{12}$$

Because we are roughly neglecting the draining stage, the value of h in Eq. (12) has to be set to the critical distance for film instability $h_c = [(AR)/(8\pi\Gamma)]^{1/3}$ [26].

By substituting Eqs. (11) and (12) into Eq. (9), the following simplified relationship for the rate of coalescence at rest is derived:

$$\frac{dR_v}{dt} \cong \frac{1}{3\eta^*}\left[\Phi\left(1 - \exp\left\{-\frac{9\Phi[AR_v]^{1/3}}{[8\pi\Gamma]^{1/3}2(1-\Phi)R_v}\right\}\right)2\sqrt[3]{2\Gamma}\right] \tag{13}$$

In the previous relationship, the Hamaker constant A is the only unknown parameter, representative of the interactions between the droplets, and it has been used as the fitting parameter during the fitting of experimental data of droplet coalescence.

The volume-average radii R_v at rest are reported in Fig. 7 for the blends as a function of time after shear flows at $\dot{\gamma} = 0.631\ s^{-1}$ and $1.585\ s^{-1}$, that are the highest shear rates of rheo-optical analyses. The solid lines of Fig. 7 were obtained by fitting Eq. (13) to the experimental data. The values of the fitting parameters A are summarized in Table 3.

An increase of R_v up to $\sim 20\%$ can be argued only for the P12 blend after submitted it to shear flows at $1.585\ s^{-1}$, while a substantial morphological stability during time emerges at the lower shear rate. Though the data at $\dot{\gamma} = 0.631\ s^{-1}$ are characterized by variations of drop size comparable with the experimental uncertainty, we note that the values of the fitting parameter A for P12 blend are similar and they do not depend on the rate of the previous shear flow, only affecting the initial drop sizes. Moreover, the values of fitting parameters are close to the typical Hamaker constant for hydrocarbons (A of order of 10^{-20} J [35]). Conversely, a great morphological stability characterizes the compatibilized blend independently on the pre-shear, or alternatively, independently on the initial drops size. By analysing the data of Table 3, we note that the

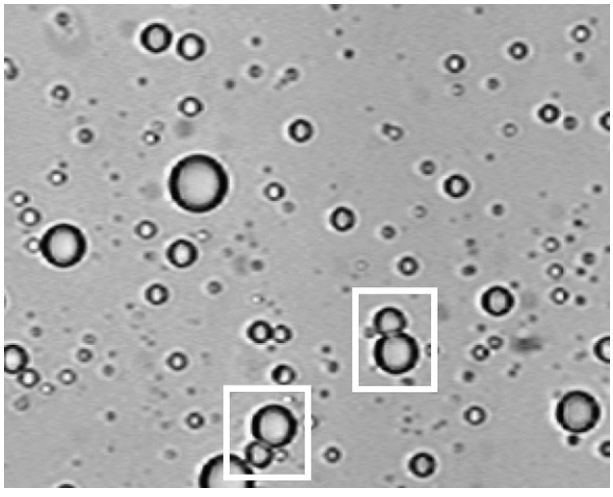

Fig. 6. Micrograph of P12 blend in the early stages of the quiescent annealing process. Two couples of contacting droplets are shown in the boxes.

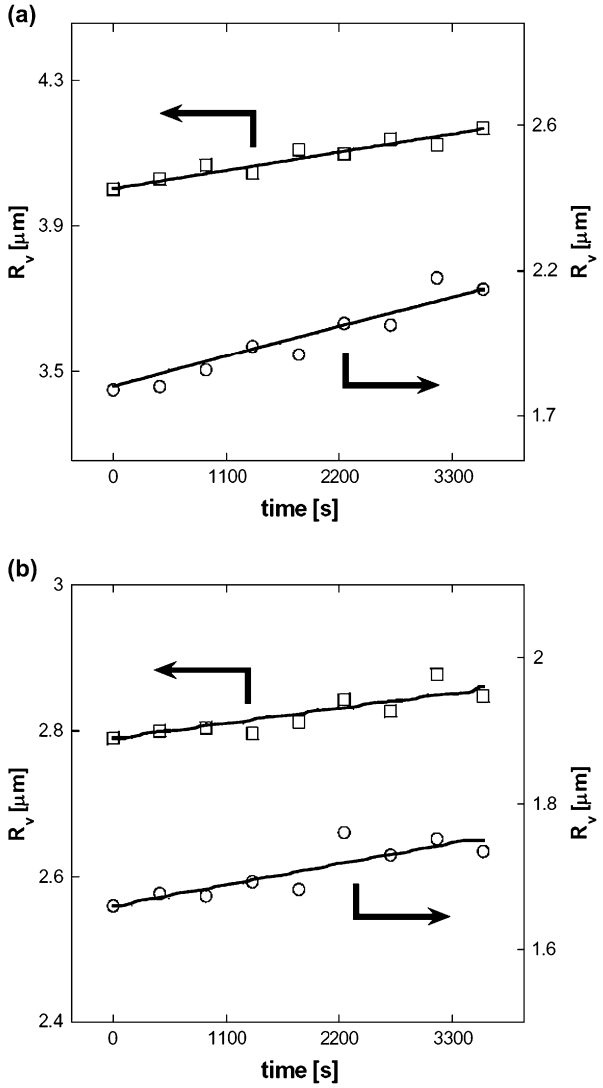

Fig. 7. Average radii at rest for P12 (a) and P12E (b) blends as a function of time. The blends were previously submitted to steady shear flows at $\dot{\gamma} = 0.631\ s^{-1}$ (□) and $\dot{\gamma} = 1.545\ s^{-1}$ (○). The solid lines represent the estimations of Eq. (13).

presence of the compatibilizer causes a decrease of A. This is probably due to the presence of the copolymer at the interface between the phases, causing a shielding effect between the dispersed phases. Finally, by investigating the dependences of the model (Eq. (13)) on their parameters, a strong dependence on both the A and the initial droplet radius has been noticed. On the contrary, a negligible dependence on the interfacial tension is emerged. The presence of the compatibilizer is mainly taken into account by the reduced values of the fitting parameter A, taking into account the interactions between the droplets. This means that smaller wall-to-wall distances ($h_c \propto A^{1/3}$) have to be reached to induce coalescence in the compatibilized blend, reducing the coalescence rate. However, it has to be stressed that the simplified model proposed does not exclude the occurrence of other mechanisms participating to coalescence suppression in the compatibilized blend.

Table 3
Fitting parameters A obtained by fitting Eq. (13) to the experimental data of $R_v(t)$

Material	Pre-shear rate (1/s)	$A \times 10^{20}$ (J)
P12	0.631	1.94
	1.585	1.89
P12E	0.631	0.384
	1.585	0.476

4. Conclusions

The relationships between flow and morphology of a diluted LDPE/PA6 blend (97/3 wt/wt) have been studied by means of rheological and rheo-optical techniques. In particular, the effects related to different flow fields and the presence of a compatibilizing agent were investigated.

The steady-state viscosity of the uncompatibilized system follows quite well the log-additivity rule, while a relevant positive deviation has been detected for the compatibilized blend. The linear viscoelastic moduli follow the same trend of the shear viscosity at high frequencies, the moduli of the blends being higher or lower than those of the LDPE matrix depending on, respectively, the presence or the absence of the compatibilizing agent. At low frequencies, however, the presence of the dispersed phase causes a slight enhancement of the blend elasticity (G'). Such effect is more relevant for the compatibilized system.

The rheo-optical analyses allowed studying the evolution of drop size distributions soon after steady shear flows at different shear rates. The qualitative analysis of drop size distributions indicates that the presence of compatibilizer causes a stabilization of blend morphology for weak flow fields. Conversely, a broadening of the drop size distributions has been detected for uncompatibilized blend at low shear rates. However, the drop sizes of both the blends decrease with increasing the shear rate. The presence of high diameter tails characterizes the uncompatibilized blend soon after a high shear rate flow. This feature has not been observed in the presence of the compatibilizer.

In order to relate more rigorously the external flow and the blend morphology, rescaling of capillary number and viscosity ratio has been performed. In particular, the shear-rate-dependent viscosities of blend constituents have been used into the classical critical curves for droplet break-up and coalescence derived for Newtonian blends. This allowed to roughly estimate the critical shear rates in order that relevant droplet break-up occur for uncompatibilized blend. Conversely, an underestimation of the equilibrium volumetric mean radius has been found for compatibilized blend, indicative of stabilization of the blend morphology in shear flow.

Finally, the coarsening behaviour during the earlier stages of a quiescent annealing process has been investigated, and a simplified model has been proposed to describe the coalescence phenomena occurring at rest. Though the experimental data are affected by poor reliability, the morphological stability emerged for compatibilized blend during a quiescent annealing could be related to some shielding effect related

to the presence of the copolymer at the interface between the phases. This should cause decreasing of the Hamaker constant of PA6 droplets on the basis of the coarsening process.

Acknowledgements

The authors are thankful to Prof. Nino Grizzuti and Dr. Stefano Acierno for the support in the using of the rheo-optical apparatus and for the useful scientific discussions. The authors are also thankful to the Italian Ministry of University and Scientific and Technological Research (MURST) (contract no. MM09244737) for the financial support.

References

[1] Utracki LA. Commercial polymer blends. London: Chapman and Hall; 1998.
[2] Minale M, Moldenaers P, Mewis J. Macromolecules 1997;30:5470.
[3] Palierne JF. Rheol Acta 1990;29:204–14. Erratum: Rheol Acta 1991;30: 497.
[4] Graebling D, Muller R. J Rheol 1990;34(2):193.
[5] Taylor GI. Proc R Soc Lond Ser A 1932;138:41.
[6] Taylor GI. Proc R Soc Lond Ser A 1934;1346:501.
[7] Grace HP. Chem Eng Commun 1982;14:225.
[8] Jansen KMB, Agterof WGM, Mellema J. J Rheol 2001;45:227.
[9] Wu Souheng. Polym Eng Sci 1987;27:335.
[10] Everaert V, Aerts L, Groeninckx G. Polymer 1999;40:6627.
[11] Fortenlý I. Polym J 2004;40:2161.
[12] Nandi A, Khakhar DV, Mehra A. Langmuir 2001;17:2647.
[13] Sundararaj U, Macosko CW. Macromolecules 1995;28:2647.
[14] Minkova L, Yordanov Hr, Filippi S. Polymer 2002;43:6195.
[15] Yordanov Hr, Minkova L. Eur Polym J 2005;41:527.
[16] Yordanov Hr, Minkova L. Eur Polym J 2003;39:51.
[17] Scaffaro R, La Mantia FP, Canfora L, Polacco G, Filippi S, Magagnini P. Polymer 2003;44:6951.
[18] Minkova L, Yordanov Hr, Filippi S, Grizzuti N. Polymer 2003;44:7925.
[19] Caserta S, Simeone M, Guido S. Rheol Acta 2004;43:491.
[20] Paine AJ. Part Part Syst Char 1993;10:26.
[21] Utacki LA. J Rheol 1991;35:1615.
[22] Utracki LA, Kamal MR. Polym Eng Sci 1982;22:96.
[23] Tucker CL, Moldenaers P. Annu Rev Fluid Mech 2002;34:177.
[24] de Bruijn RA. PhD thesis, Eindhoven University of Technology; 1989.
[25] Chesters AK. Int J Multiphase Flow 1975;2:191.
[26] Chesters AK. Euromech 234 – International conference on turbulent two phase flow systems. Touluse, France; 1988.
[27] Mackay GDM, Mason SG. Can J Chem Eng 1963;41:203.
[28] Hudson SD, Jamieson AM, Burkhart BE. J Colloid Interface Sci 2003;265:409.
[29] Lyu SP, Jones TD, Bates FS, Macosko CW. Macromolecules 2002;35: 7845.
[30] Yu Wei, Zhou Chixing, Inoue Takashi. J Polym Sci Part B Polym Phys 2000;38:2378.
[31] Fortenlý I, Źivný A, Jůza J. J Polym Sci Part B Polym Phys 1998;37:181.
[32] Barnes HA, Hutton JF, Walters K. An introduction to rheology. Amsterdam, The Netherlands: Elsevier Science Publishers B.V.; 1989.
[33] Nauman EB, He DQ. Chem Eng Sci 2001;56:2000.
[34] Fortenlý I, Źivný A. Polymer 1995;36:4113.
[35] Israelachvili J. Intermolecular and surface forces. London: Academic Press; 1992.